GEOPHYSICS, VOL. 63, NO. 3 (MAY-JUNE 1998); P. 826–840, 22 FIGS.

Marine magnetotellurics for petroleum exploration, Part II: Numerical analysis of subsalt resolution

G. Michael Hoversten*, H. Frank Morrison*, and Steven C. Constable‡

ABSTRACT

In areas where seismic imaging of the base of salt structures is difficult, seaborne electromagnetic techniques offer complementary as well as independent structural information. Numerical models of 2-D and 3-D salt structures demonstrate the capability of the marine magnetotelluric (MT) technique to map the base of the salt structures with an average depth accuracy of better than 10%. The mapping of the base of the salt with marine MT is virtually unaffected by internal variation within the salt. Three-dimensional anticlinal structures with a horizontal aspect ratio greater than two can be interpreted adequately via two-dimensional inversions. Marine MT can distinguish between salt structures which possess deep vertical roots and those which do not.

One measure of the relative accuracy of MT and seismic methods can be made by considering the vertical and lateral position errors in the locations of interfaces caused by neglecting velocity anisotropy in migration. For the shallow part of the section where two-way travel times are on the order of 1 s, the vertical and lateral position errors in the locations of salt-sediment interfaces from 2-D MT inversion is more than twice the expected migration error in reflectors in transversely isotropic sediments, such as those in the Gulf of Mexico. Deeper in the section where two-way times are on the order of 4 s, lateral position errors in migration become comparable to those of the MT inverse, whereas seismic vertical position errors remain more than a factor of two smaller than MT errors. This analysis shows that structural mapping accuracy would be improved using MT and seismic together.

INTRODUCTION

Seismic imaging beneath high-velocity and often inhomogeneous formations is a formidable task, even with the most comprehensive 3-D seismic surveying techniques. Basalts and carbonates commonly pose difficulties for reflection surveys because excessive reverberations effectively mask reflections from structures beneath them. Similarly, salt structures contain entrained sediments that produce significant scattering and, in addition, have strong reflecting vertical boundaries that strain the limits of 3-D migration. As a result, ambiguities in the interpretation of seismic reflection data often remain, even in 3-D surveys. Finally, there are many practical exploration problems where it is important to test a relatively simple hypothesis before deciding if the expense of a full 3-D seismic survey is warranted.

Electrical resistivity provides important complementary information in these situations. The resistivity of salt and of basalts and carbonates is often more than ten times greater than the surrounding sediments. With such contrasts, magnetotellurics (MT) can easily map major structures and resolve the ambiguities noted above. In practice, the applicability of MT spans the range from stand-alone techniques for resolving gross structure to sophisticated joint applications where structure derived from seismic is essential for fixing some of the parameters in the electrical model of the subsurface. The effective resolution of MT depends entirely on the constraints that can be imposed on the interpretation by other data. Interpreted alone, MT data can give only a gross description of the section. The more information that can be provided from seismic data (for interface depths, location of faults, etc.), drillhole data, or gravity, the better the accuracy of the resulting conductivity cross-section.

While marine MT can independently provide structural interpretations of lateral salt intrusions in the Gulf of Mexico (GOM) in seismic no-record areas, it is best used in conjunction with existing seismic data. The seismic data can define the structure down to the top of the salt, allowing these parameters

Presented at the 66th Annual International Meeting, Society of Exploration Geophysicists. Manuscript received by the Editor May 31, 1996; revised manuscript received March 31, 1997.
*Lawrence Berkeley Natl. Lab., 1 Cyclotron Road, Berkeley, CA 94720. E-mail: mhovers@socrates.berkeley.edu.; hfmengeo@socrates.berkeley.edu.
‡Scripps Institution of Oceanography, IGPP 0025, 8604 La Jolla Shores Drive, LaJolla, CA 92093-0225; E-mail: sconstable@ucsd.edu.

to be fixed at known values in the marine MT inversions, resulting in improved base salt structure. In deep exploration where velocity estimation for migration is inherently problematic, the marine MT resistivity structure, when used with velocity-resistivity relations derived from log information, can provide independent velocity estimates that can constrain the possible migration velocities.

Figure 1 shows a depth-converted seismic section for the GOM. In this example coherent reflections exist beneath the top of the salt which can be interpreted, but uncertainty exists as to which reflector represents base of the salt. As we will demonstrate, the accuracy of marine MT interpretations would determine which seismic event corresponded to the base of the salt.

The idea of using electromagnetic (EM) techniques, including MT, on the ocean bottom for petroleum exploration is not new. Mobil Oil first tried MT in shallow water of the Gulf of Mexico in the late 1950s (Hoehn and Warner, 1960). The Mobil experiment suffered from two major problems. First, the shallow water depth of 20 m resulted in significant wave motion of the magnetic field sensors. Second, MT data processing in the late '50s did not use the remote reference techniques pioneered by Gamble et al. (1979). The remote reference technique reduces the systematic bias in impedance estimates. Controlled-source EM techniques have been studied for decades (e.g., Chave et al., 1991; Constable et al., 1986; and Edwards, 1988) for probing the deep ocean crust and for their potential applications for mineral and petroleum exploration. Studies of the relative effectiveness of controlled-source EM systems and marine MT in terms of 2-D inverse model resolution of salt structures has been presented by Hoversten (1992) and Hoversten and Unsworth (1994). We focus on MT rather than controlled source because we feel the logistics of using a controlled source will result in higher survey costs compared to MT.

THE SYSTEM

A useful review of the general MT method is given by Vozoff (1991), and the effect of the sea water layer on impedance measurements on the ocean bottom is summarized in a companion paper by Constable et al. (1998, this issue). The data used in our inversions are the apparent resistivity and phase defined for a 1-D earth in Constable et al. (1998, this issue).

The source or incident fields for MT measurements in the 10^{-3} to 1.0 Hz band (the frequencies of interest for marine MT) can be considered to be the horizontal components of the magnetic field. All measured fields, electric E and magnetic H, can then be considered to be produced by induction via linear transfer functions, T, from these horizontal components. In the most general case, within an inhomogeneous medium, these relations can be written in the form of the matrix transfer function:

$$\begin{vmatrix} \mathbf{E}_x^{Obs.} \\ \mathbf{E}_y^{Obs.} \\ \mathbf{E}_z^{Obs.} \\ \mathbf{H}_x^{Obs.} \\ \mathbf{H}_y^{Obs.} \\ \mathbf{H}_z^{Obs.} \end{vmatrix} = \begin{vmatrix} \mathbf{T}_1 & \mathbf{T}_2 \\ \mathbf{T}_3 & \mathbf{T}_4 \\ \mathbf{T}_5 & \mathbf{T}_6 \\ \mathbf{T}_7 & \mathbf{T}_8 \\ \mathbf{T}_9 & \mathbf{T}_{10} \\ \mathbf{T}_{11} & \mathbf{T}_{12} \end{vmatrix} \bullet \begin{vmatrix} \mathbf{H}_x^{Inc.} \\ \mathbf{H}_y^{Inc.} \end{vmatrix} \tag{1}$$

Where $H^{Inc.}$ represents the incident magnetic fields on the sea surface. One can form the two relations;

$$\begin{vmatrix} \mathbf{E}_x^{Obs.} \\ \mathbf{E}_y^{Obs.} \end{vmatrix} = \begin{vmatrix} \mathbf{T}_1 & \mathbf{T}_2 \\ \mathbf{T}_3 & \mathbf{T}_4 \end{vmatrix} \bullet \begin{vmatrix} \mathbf{H}_x^{Inc.} \\ \mathbf{H}_y^{Inc.} \end{vmatrix} \tag{2}$$

and

$$\begin{vmatrix} \mathbf{H}_x^{Obs.} \\ \mathbf{H}_y^{Obs.} \end{vmatrix} = \begin{vmatrix} \mathbf{T}_7 & \mathbf{T}_8 \\ \mathbf{T}_9 & \mathbf{T}_{10} \end{vmatrix} \bullet \begin{vmatrix} \mathbf{H}_x^{Inc.} \\ \mathbf{H}_y^{Inc.} \end{vmatrix} \tag{3}$$

Rearranging equation (3) for the incident fields and substituting into equation (2) yields:

$$\begin{vmatrix} \mathbf{E}_x^{Obs.} \\ \mathbf{E}_y^{Obs.} \end{vmatrix} = \begin{vmatrix} \mathbf{T}_1 & \mathbf{T}_2 \\ \mathbf{T}_3 & \mathbf{T}_4 \end{vmatrix} \bullet \begin{vmatrix} \mathbf{T}_7 & \mathbf{T}_8 \\ \mathbf{T}_9 & \mathbf{T}_{10} \end{vmatrix}^{-1} \bullet \begin{vmatrix} \mathbf{H}_x^{Obs.} \\ \mathbf{H}_y^{Obs.} \end{vmatrix} \tag{4}$$

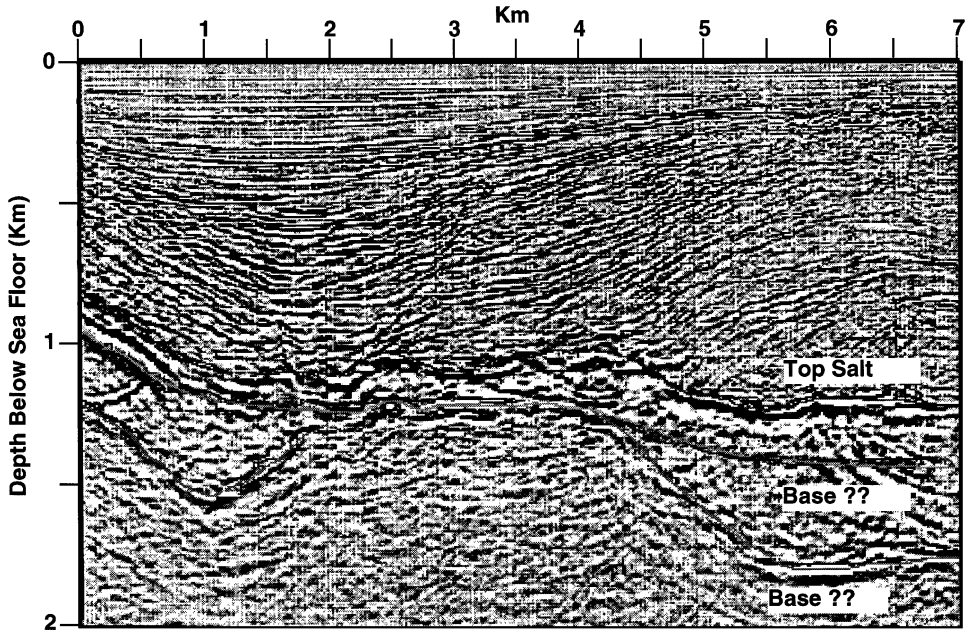

FIG. 1. Depth-converted seismic line from offshore GOM showing two possible base salt interpretations.

Equation (4) shows that even within the medium, the orthogonal E and H components can be related by a 2×2 impedance tensor.

MT interpretation depends on the construction of models of the subsurface conductivity distribution which reproduce the observed impedance (or, alternatively, the apparent resistivity and phase) at the measurement point. Papers by Smith and Booker (1988) and deGroot-Hedlin and Constable (1990) are examples of numerical inversion processes for effecting this interpretation.

As pointed out in Part 1, Constable et al. (1998, this issue), if the section is horizontally layered, it is an interesting property of the plane-wave impedance that the ocean-bottom impedance is the surface impedance of the earth, as if the ocean were not present. If the earth is inhomogeneous, this is not the case and the models and inversion codes must account for the overlying ocean. We have used the general 2-D code of Wannamaker (1987), which generates impedances on the ocean bottom.

MODELS AND MODELING

In this paper we will consider two sample models. The first is the anticlinal structure shown in Figure 1. Seismic reflections may or may not be evident from the base of the salt structure. When reflections are present, ambiguity may exist as to which reflector represents the base of salt. Our first model introduces the algorithms used and illustrates the resolution on the base of the salt for anticlinal structures. A second type of salt structure is that in which the presence or absence of a deep-seated root is of critical interest. This problem is addressed by comparing inversions of a salt structure with and without a deep root.

A partial survey of deep induction logs from wells that penetrate salt in the GOM show sediment resistivities range from 0.25 to 2 ohm-m while salt resistivities can range from 10 to 1000 ohm-m. The low salt resistivities result from intermixing with sediment during emplacement. The high salt resistivities represent massive salt. Figure 2 shows a portion of a typical deep induction log from a well penetrating salt in the GOM. In all the models illustrated in this paper, we have used a sediment resistivity of 1 ohm-m and a salt resistivity of 20 ohm-m.

The presence of oil in sediments raises their resistivity to between 10 and 20 ohm-m. If the salt acted as a structural trap with oil just beneath the salt, the ability to distinguish between salt and oil-bearing sediment would be a problem. Fortunately, many if not all of the subsalt discoveries to date have involved oil and gas located substantially below the salt, with a large enough section of low-resistivity sediment beneath the salt to allow the base of salt to be distinguished.

The development of accurate numerical modeling algorithms for 2-D and 3-D structures has made great strides in the last decade. It is now possible to calculate the MT response of 1-D, 2-D, and 3-D structural models of interest to the petroleum industry. In addition (2-D and 3-D) MT inverse technology is improving rapidly. For the MT examples, we have used the forward 2-D MT modeling algorithm of Wannamaker (1987), the forward 3-D MT modeling algorithm of Mackie et al. (1993), and the 2-D MT inverse of deGroot-Hedlin and Constable (1990).

2-D salt anticline

Figure 3 shows a 2-D salt model whose style is taken from the seismic section of Figure 1. The sedimentary section is beneath 300 m of 0.3-ohm-m sea water. The slopes on either side of the anticline differ by a factor of two to investigate the lateral resolution of marine MT. The salt layer contains a random distribution of inclusions of both high and low resistivity representing zones of included sediment or massive salt. The MT apparent resistivity versus frequency for the model of Figure 3 is compared to that for a homogeneous salt body with the same structure in Figure 4 . Figure 4 demonstrates the insensitivity of MT to variations in the resistivities within a resistive structure such as the salt. This occurs because the MT response at these frequencies is totally dominated by the effects of electric currents channeled around the resistive salt and into the core of the anticline. There is very little change in response as the resistivity contrast between a resistive target and its surroundings

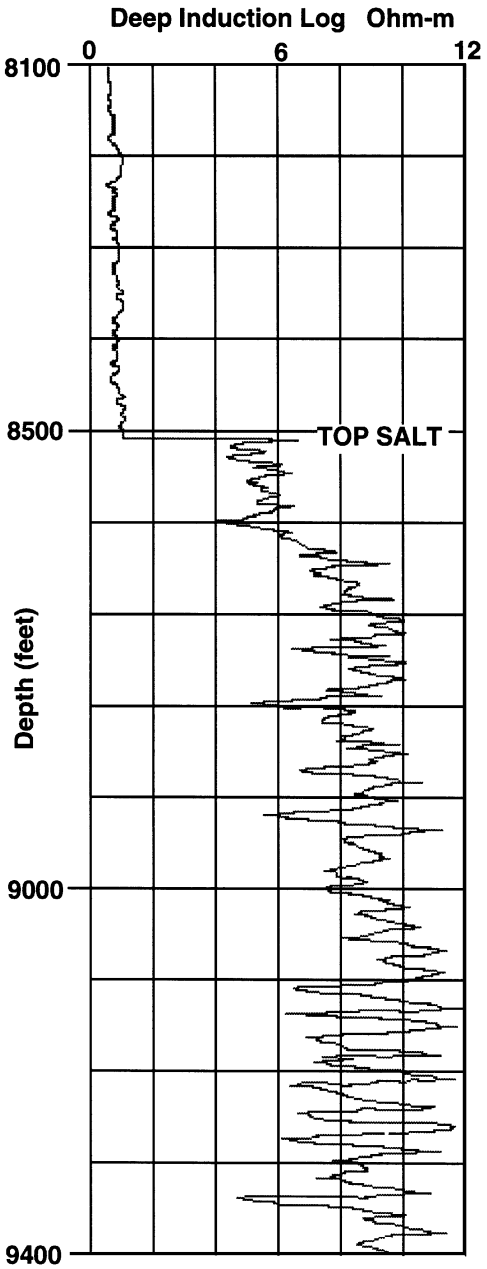

FIG. 2. Portion of a deep induction log from offshore GOM showing salt and sediment resistivities.

increases beyond a ratio of 10:1 because the contribution of induced currents within the resistive structure is negligible. This is very beneficial for the inversion of such data because internal variations in the salt have little or no effect on the data.

SPATIAL VARIATIONS OF MAGNETIC FIELDS IN MARINE MT

Marine MT differs significantly from land MT if the section below the sea floor is inhomogeneous. At the air-ground interface the boundary condition requires that there be no vertical component of current and consequently no vertical electric field, E_z. This is not a requirement at the ocean bottom interface, so vertical electrical field measurement may be a useful additional measurement for marine MT. The presence of E_z, which varies spatially, also changes some assumptions about the behavior of the horizontal magnetic fields in surface MT surveys.

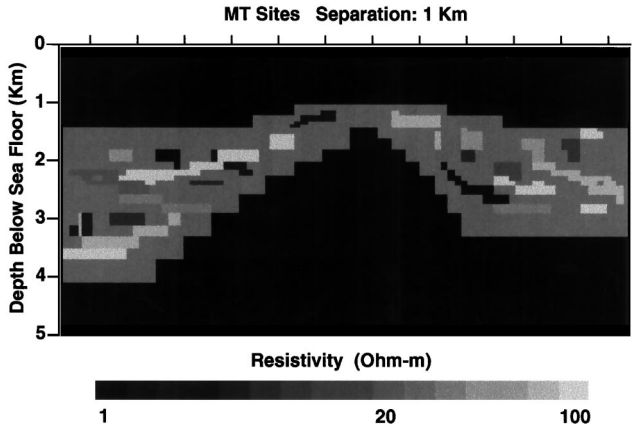

FIG. 3. Two-dimensional numerical salt anticline model. The sediment resistivity is 1 ohm-m and the salt resistivity is 20 ohm-m. Within the salt structure are large inclusions, ranging in resistivity from 1 ohm-m representing sediment to 100 ohm-m and representing nearly pure salt.

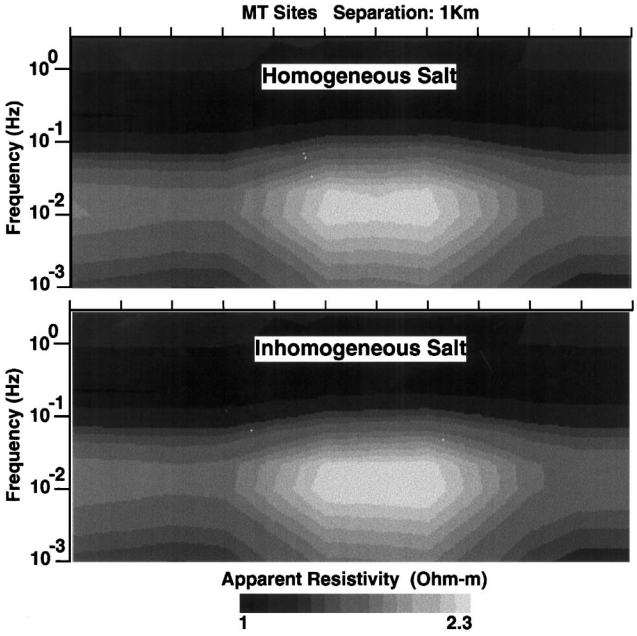

FIG. 4. TM mode (E field perpendicular to strike) apparent resistivity for 2-D anticline model shown in Figure 3 with and without the inclusions within the salt. Only a very minor difference is caused by the inclusions beneath site 7.

For example, in a 2-D medium in which the properties are constant in the y-direction (the strike direction), a plane wave incident with a magnetic field polarized in the y-direction (the TM mode) must have a constant H_y value in the x-direction. This is a consequence of $\bar{\nabla} \cdot \bar{H} = \bar{J}$, where J is current. The vertical current, J_z, is given by

$$\frac{\partial H_y}{\partial x} - \frac{\partial H_x}{\partial y} = J_z.$$

Since H_x is zero by definition of the incident field and J_z is zero from the boundary condition, H_y must be a constant. However, at the sea-floor interface J_z is not zero, so H_y can be a function of x. On the sea floor then, both H_x and H_y are functions of position, even for 2-D geology. Profiling techniques such as electromagnetic array profiling (EMAP) (Torres-Verdin and Bostick, 1992), which are normally interpreted assuming transverse magnetic (TM) mode data with constant H, must be considered differently for sea-floor surveys.

To illustrate the magnitude of these new features of marine MT, we have calculated the transverse electric (TE) and TM mode apparent resistivities over the anticlinal model of Figure 3 with and without the sea water layer. The ratio of TE apparent resistivity without sea water to the TE apparent resistivity with sea water is shown in the top panel of Figure 5, and the TM apparent resistivity ratio is shown in the bottom panel of Figure 5. The TM without/with anomaly is pronounced and reaches 18% over the anticline, while the maximum TE without/with ratio is only 2%.

When we consider the spatial variation across the anticline of the H_y and E_x fields (TM impedance) caused by the sea water, we find that the maximum spatial variation in H_y across the anticline is approximately 11% at 0.1 Hz. The H_y variation with frequency decreases to approximately 5% at 0.001 Hz. The maximum spatial variation in E_x is approximately 10% at 0.1 Hz and increases to nearly 15% at 0.001 Hz. This indicates (1) the variation of H_y due to the presence of the sea water is a significant component in the differences in TM apparent resistivity shown in Figure 5 and (2) the common assumption that both horizontal components of H are for practical purposes constant over the surface of a half-space is probably not safe for ocean bottom measurement.

SALT ANTICLINE

1-D inversion of 2-D salt anticline

Two-dimensional structures such as the one shown in Figure 3 can be reasonably interpreted using 1-D inversion of the mode in which E is parallel to strike (TE mode) because, with the exception of the core of the anticline, the E parallel to strike is only slightly perturbed from the 1-D response. The two most popular techniques for 1-D inversion are (1) a least-squares inversion of a sparse layered model and (2) a smooth Occam inversion (Constable et al., 1987). Figure 6 shows a 1-D Occam model that fits the TE apparent resistivity and phase at site 2 of the 2-D anticline model (without inclusions) shown in

Figure 3. The 1-D Occam inversion assumes no prior knowledge about the model. The starting model is a half-space of 1 ohm-m. The portion of the inverted model between 1000 and 4000 m depth above 2 ohm-m represents the salt. However, two artificial high regions above and below the salt manifest themselves in the unconstrained 1-D model.

Figure 7 shows the results of doing 1-D Occam inversions of the TE apparent resistivity and phase at all sites, separated by 1 km, along the model shown in Figure 3 (without inclusions). On the flanks of the anticline, the 1-D models do a reasonable job of imaging the base of the salt. However, at the core of the anticline where the TE currents are concentrated by the structure, the TE apparent resistivities are elevated, resulting in 1-D models with a thicker section of high resistivity (salt) than is present in the 2-D model.

Smooth inverse models, whether 1-D or 2-D, have an inherent drawback when used to interpret geology that contains sharp discontinuities in physical properties. A resistivity contour must be picked to represent the location of the sharp physical discontinuity, such as the base of the salt. The choice of which resistivity contour to use must be guided by the inversion of numerical model data and by choosing the contour of the resulting inversions that most closely approximates the correct position of the discontinuity.

For problems where information is available from other geophysical methods, such as seismic or gravity, a technique that can accommodate this information as constraints on the inversion is preferable. A 1-D inversion that uses only three layers and in which the depth to the top of the salt and the resistivities of the sediment and salt can be fixed yields a more accurate estimate of the salt thickness. Figure 8 presents the three-layer 1-D inversion of the 2-D salt anticline model. The average error in the depth to the base of the salt beneath the MT sites is 13.2% for the three-layer inversions shown in Figure 8 and 16.2% for the Occam inversions shown in Figure 7. In addition, the three-layer inversion error in the anticline apex thickness is 10% better than the unconstrained Occam estimate.

2-D inversions of 2-D salt anticline

While the 1-D inversions can be used as a fast first pass at data modeling, additional accuracy can be gained by using a

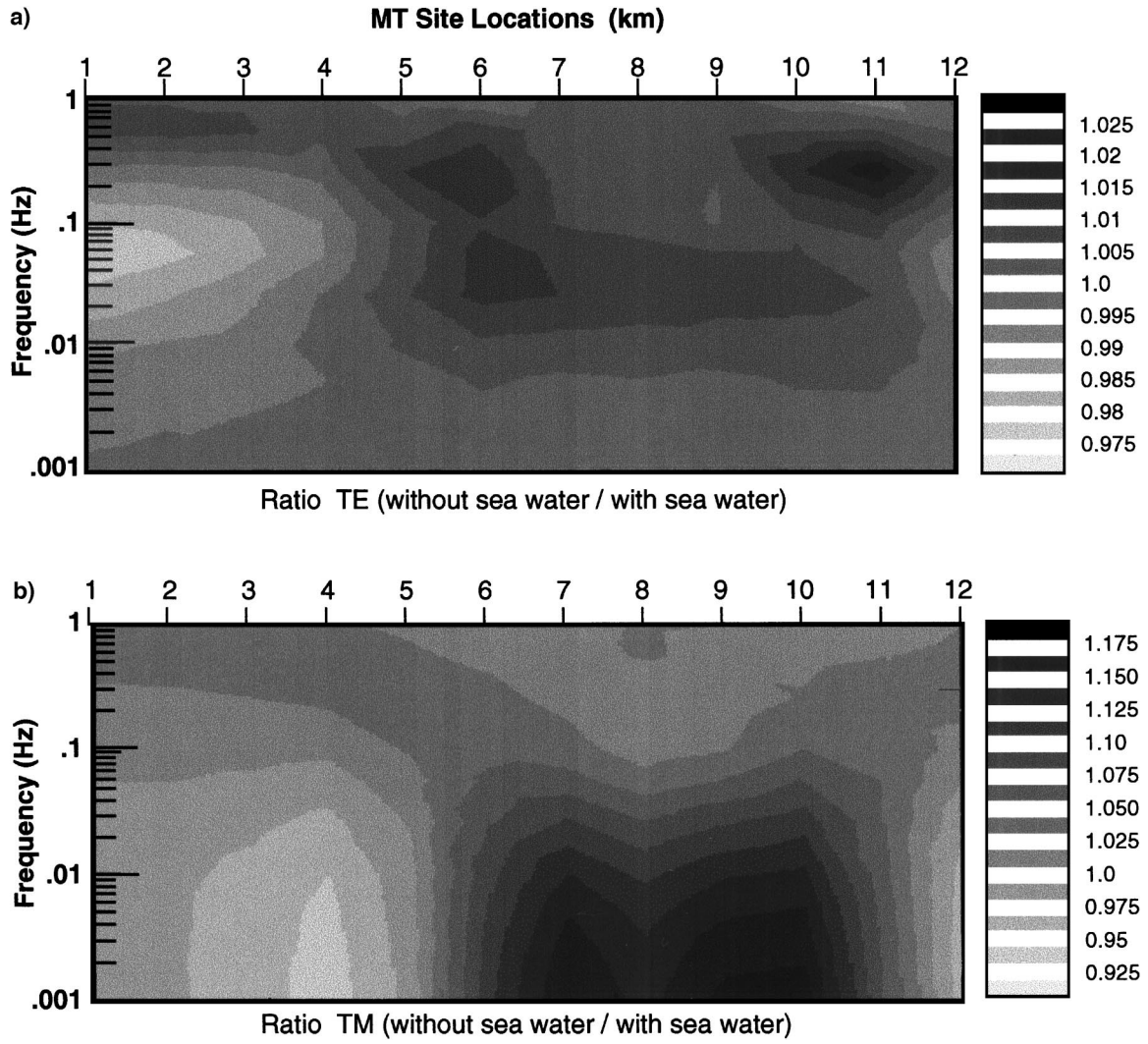

FIG. 5. Numerical results of salt anticline model without sea water divided by results with sea water. Panels show the ratio of TE (a) and TM (b) apparent resistivities for the model shown in Figure 3 (no inclusions).

full 2-D solution. The 2-D inversions were done assuming the structure to the top of the salt would be constrained by seismic data; hence, the resistivity and structure were held constant to the top of the salt. The starting model was a half-space of 1 ohm-m sediment with 300 m of overlying sea water.

For 3-D structures, which have surface topography out of the plane of a 2-D inversion, fixing the top structure may actually degrade the accuracy of the base salt from a 2-D inversion. The appropriateness of fixing the top structure is model dependent and must be judged based on modeling results for a particular situation.

Thirteen MT sites, spaced 1 km apart, were used with ten equally spaced frequencies in the $\log^{10}$ domain from 1.0 to 0.001 Hz. Figure 9 shows the MT inverse model when both TE and TM mode apparent resistivity and phase data were used with 5% random noise added. The true model structure is shown in white. To quantitatively interpret the inverse models for the base of the salt, a resistivity contour which most closely matches the true base of salt must be chosen—in this example, the 3.2-ohm-m contour. The percent error plotted in the top panel of Figure 9 is the percent difference between the true model and the depths of the 3.2 ohm-m contour, shown in the middle panel, calculated at the MT sites. The errors on the flanks of the anticline are near 5%. Across the apex of the structure they increase to a maximum of 14%. The average base salt depth error is 8% across the entire model.

The bottom panel of Figure 9 shows the complete smooth resistivity distribution recovered by the Occam 2-D inversion. The granularity of the resistivity represents the size of the regularization mesh, which defines the blocks of constant resistivity which are the inversion parameters. The regularization mesh was generated without any attempt to match regularization mesh boundaries to boundaries in the true model. As a result, most of the regularization mesh blocks straddle the salt-sediment boundaries in the true model. An exception occurs beneath site 6, where the regularization mesh boundary falls within 100 m of the true model boundary. At this location the error is a minimum. In general, the depth of the 3.2 ohm-m contour is within one regularization mesh block of the true depth.

The observed and calculated TE and TM apparent resistivity data for the 2-D inversion shown in Figure 9 is shown in Figure 10. The area of greatest data misfit occurs at the apex of the anticline in the TE mode around 0.02 Hz where the TE apparent resistivity is most distorted by the 5% random noise. This translates into the increased base salt errors seen in the

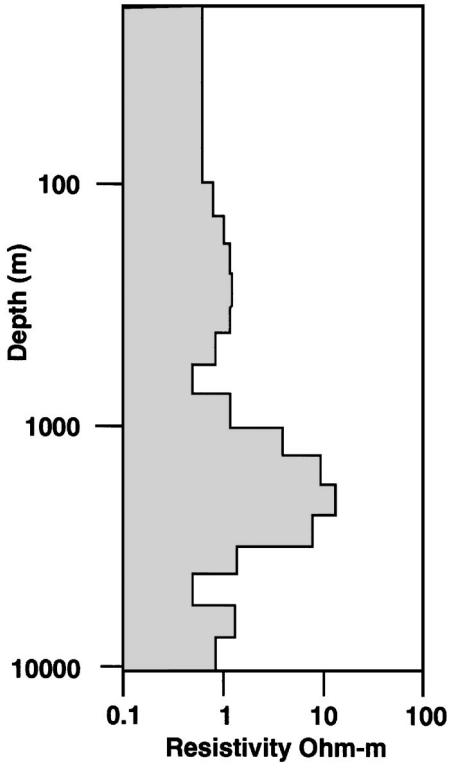

FIG. 6. One-dimensional Occam inversion of TE (*E* parallel to strike) at site 2 of the salt anticline model without inclusions shown in Figure 3.

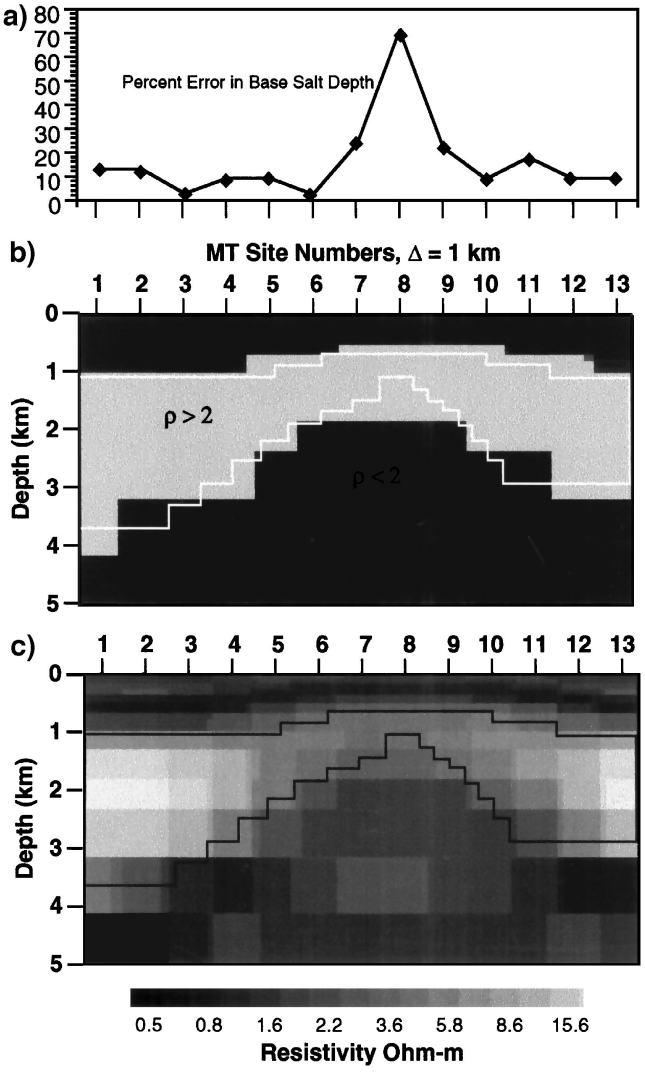

FIG. 7. (c) The stitched-together Occam 1-D TE mode inversions of Figure 3 data without inclusions and with 5% random noise added. (a) Error in the base salt estimates when the 2-ohm-m contour (shown in the middle panel) of the smoothed 1-D models is chosen as the base salt.

inverse model across the apex. When the data noise is reduced to 1%, the resulting inverse model base salt error from the 3.2 ohm-m contour drops below 5% across the apex, with an average of 6% across the entire model.

The main factor controlling the improved accuracy of the 2-D inversion compared to the 1-D inversions is the ability to fit both modes simultaneously. When 2-D inversion is done using only one mode, the errors on base salt depth are only approximately 10% better than the 1-D inversions.

2-D inversion of 3-D salt anticline

To partially address the question of the applicability of 2-D inverses to 3-D problems, the numerical 3-D anticline in a salt sheet shown in Figure 11 was constructed. The anticline has steep, 45° slopes on three sides and a more gentle 22° slope on one side. Three MT lines are simulated across the structure. Only the TM mode data were used for 2-D inversion in this example because they are least affected by the out-of-plane 3-D structure. The three inversions done as before are shown in Figure 12. The numerical solutions from the 2-D algorithm and the 3-D finite-element solutions of an elongated strike model with the same cross-section as the 2-D model differed by nearly 5%. No additional random noise was added to the 3-D data before inversion using the 2-D code.

Taking the 3.2-ohm-m contour as our estimate of the base of the salt in the inverse models, we see that for line 3 across the center of the structure the thickness estimates are less accurate than for the truly 2-D model where both TE and TM modes can be used. The data are responding to the closure of salt, which is out of the plane of the 2-D interpretation. Line 2, which is right on the edge of the 3-D crest, yields the same depth estimates as line 3. However, qualitatively we see that the resistivities within the salt are lower in the center of the structure than at its edge, giving an indication of the relative proximity to the out-of-plane edge. Line 1 lies just off the 3-D structure and predicts the salt sheet thickness to within 5%. The loss of information at the end sites is indicated by the gradations in resistivities to lower values at the ends.

The 3-D structure shown in Figure 11 has a horizontal aspect ratio, $x : y$, of 1:1 at its base which grades to 1:2 at the top. This model was stretched in the y-direction by a factor of two, and the resulting data for line 3 were inverted. The result is shown in Figure 13. The 2-D inversion of the 3-D data now recovers the structure as well as 2-D inversion of the TM mode, only over a truly 2-D model. The errors in the base salt depths are around 5% on the flanks and reach a maximum of 40% at the edge of the anticline apex.

This modeling indicates 3-D structures need only have horizontal aspect ratios greater than 2:1 to justify the use of 2-D TM mode inversion.

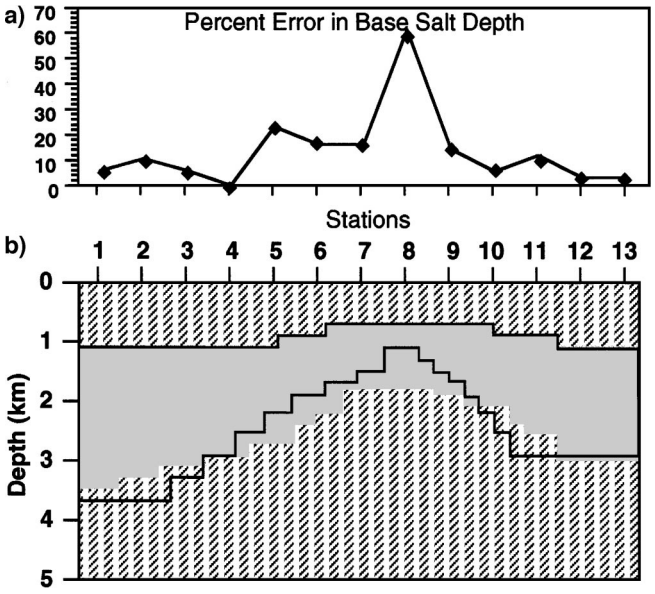

FIG. 8. (b) Stitched-together three-layer least squares 1-D TE mode inversions of Figure 3 data without inclusions and with 5% random noise added. (a) Errors in the base salt of the second layer (shown in gray in the bottom panel). The depth to the top of the salt was fixed at the correct values in the 1-D inversions.

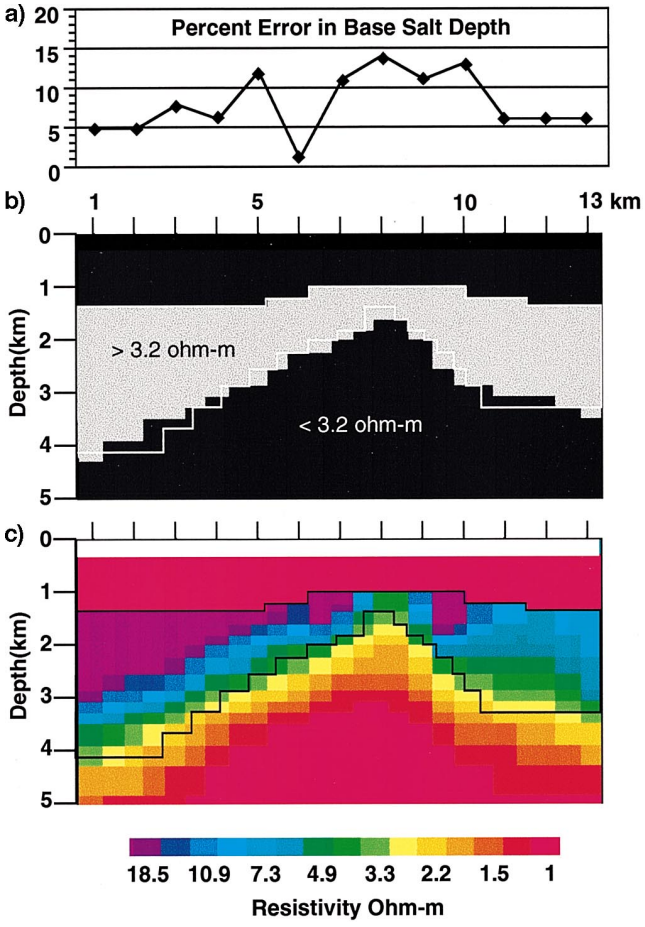

FIG. 9. Results for a 2-D Occam inversion of the data from the anticline model shown in Figure 3 (without inclusions) with 5% random noise added. (a) shows the errors in the base salt depths from picking the 3.2-ohm-m contour (b) as the base salt from the smooth inversion shown in (c). The sediment resistivity to the top of the salt was held fixed at 1 ohm-m, assuming the top salt was constrained by seismic information.

ROOTED SALT STRUCTURE

TE and TM mode responses of rooted salt structure

A second problem of interest is whether a particular salt structure possesses a deep root. The question of the presence of a root can be difficult to answer with seismic data because the overlying salt intrusion can mask the signature of the root as well as the signature of terminating beds. In addition, roots with near-vertical walls yield a seismic response that requires extremely long offsets for migration to correctly position the near-vertical reflectors. The use of gravity data can also be problematic if the salt-sediment density crossover point falls within the depth range of the root. In cases where seismic and gravity provide ambiguous interpretations of deep root structures, marine MT can provide an additional independent interpretation.

We constructed 2-D and 3-D versions of a salt structure with and without a deep root. The model is taken from an actual structure in the Gulf of Mexico. The cross-section of the structure in the x-z plane is outlined in black in Figure 15. Three 3-D versions of this model were constructed with strike lengths of 24, 16, and 12 km, respectively, in the y-direction. Before considering the 2-D inversions of the numerical data, we will consider some aspects of the MT response of such a structure. We will refer to two portions of the structure by name. The portion

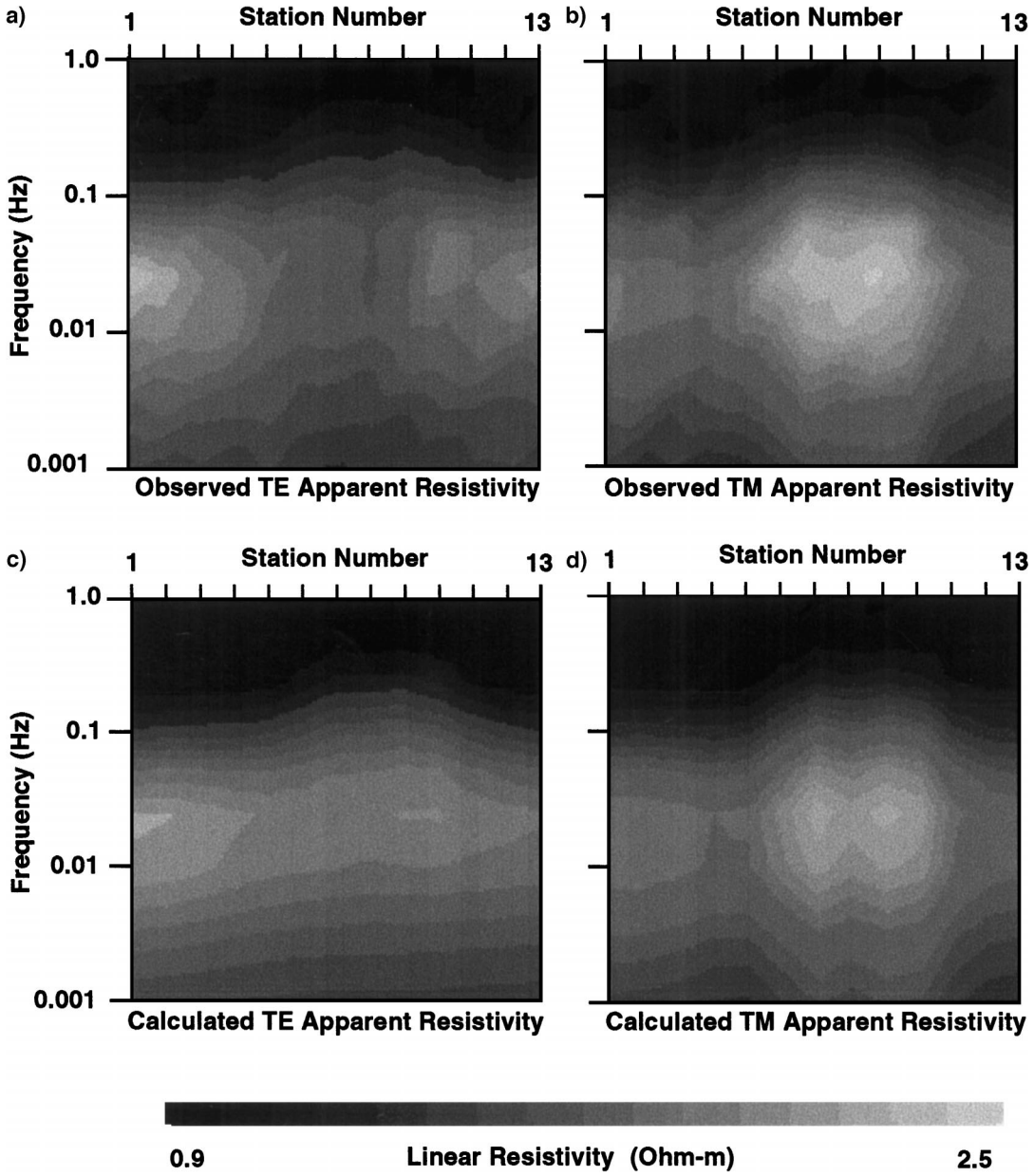

FIG. 10. Computed and observed TE and TM apparent resistivities for the inversion shown in Figure 9. (a) Observed TE apparent resistivity; numerical data from the model in Figure 3 without inclusions and with 5% random noise added. (b) Observed TM apparent resistivity; numerical data with 5% random noise added. (c) Calculated TE apparent resistivity for the inverse model shown in Figure 9. (d) Calculated TM apparent resistivity for the inverse model shown in Figure 9.

between 3 and 5 km depth and −12 to +2 km in X will be referred to as the *sill* and the portion below 5 km depth will be referred to as the *root*.

The TM (Z_{xy}) and TE (Z_{yx}) apparent resistivities for the 2-D version of the rooted and rootless salt structure are shown in Figure 14. There are three main points to be noticed regarding the response of the rooted and the rootless models:

1) The magnitude of the TM response is approximately five times larger than the TE response.
2) The TE response is more sensitive to the presence of the sill portion of the structure. This is shown by the spatial variation of the TE apparent resistivity and phase (not shown) between −10 and 0 km as compared to the TM mode data.
3) The TE response is almost completely insensitive to the root, as seen by comparing Figures 14c and 14d.

2-D inversion of 2-D rooted salt structure

The 2-D inversions of the rooted and rootless salt model data were done in the same manner as the 2-D anticline examples. Only the portion of the model below the top of the salt was inverted. All data had 5% Gaussian random noise added, and the inversions were all started from a 1-ohm-m half-space. Both TE and TM mode apparent resistivity and phase was used at ten frequencies equally spaced in $\log^{10}$ from 1 to 0.001 Hz. The inversion blocks of the model were 0.5 km wide and deep, equal to one-half a station separation, just beneath the top of the salt. Their width remained constant over the depth range of the structure, but their thickness increased with depth. Figure 15 shows the 2-D Occam inversion of the rootless structure; Figure 16 shows the 2-D Occam inversion of the rooted structure.

The outline of the rooted salt structure is overlaid in black on both figures. The lower panel has the 2-D Occam inversion of the 5% noise data as resistivity above and below 3.4 ohm-m. The upper panel shows the actual smooth Occam 2-D inverse model. The observed (numerical + 5% Gaussian noise) and calculated TM apparent resistivity and phase are shown in Figure 17 for the final inverse model with an rms misfit of 1.0. The TE mode data fits are comparable.

The 2-D inversions of rooted and rootless models show a number of things. First, the difference in the inverse models shown in Figures 15 (no root) and 16 (rooted) is a striking indication that the presence or absence of a deep root can be

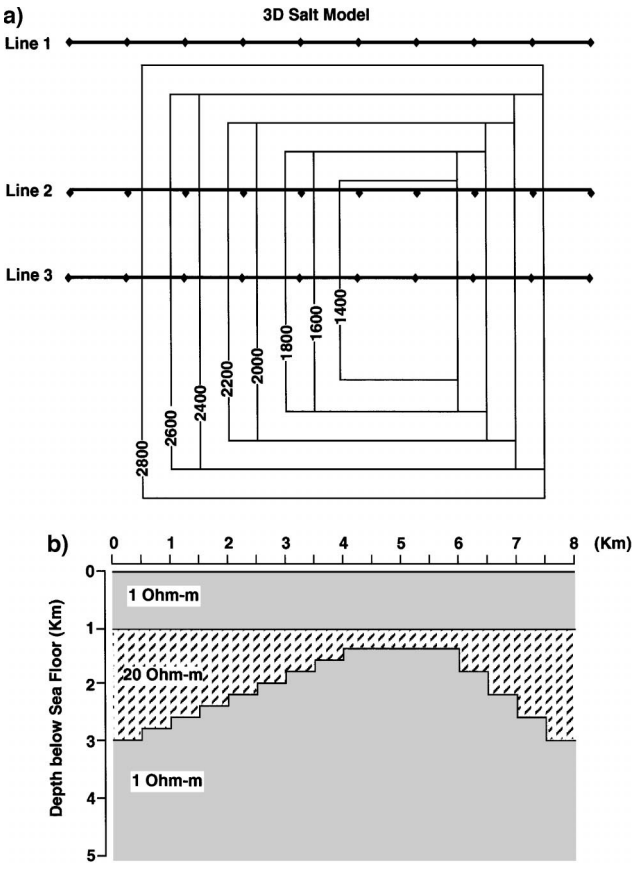

FIG. 11. Three-dimensional salt anticline model. (a) Plane view of structure. (b) Cross-section view. Numerical data were generated along three lines marked lines 1 through 3 for inversion using the 2-D Occam inverse.

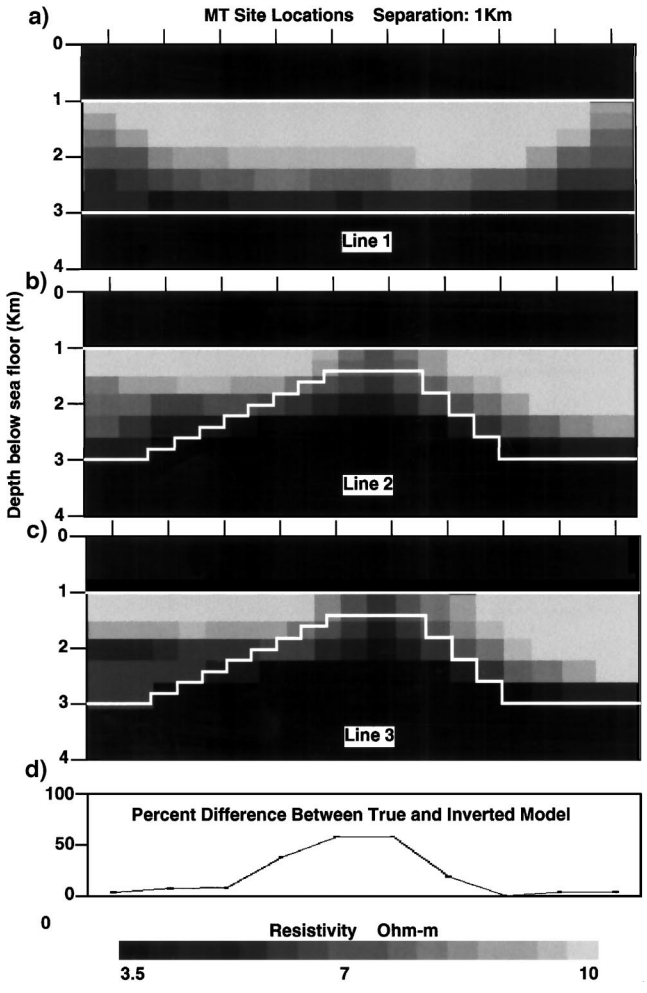

FIG. 12. Two-dimensional Occam inversion models of TM mode only for lines 1 through 3 shown in Figure 11. (a) Line 1. (b) Line 2. (c) Line 3. (d) Percent error in the depth of the base salt on lines 2 and 3 from picking the 3.2-ohm-m contour of inverse models as the base salt.

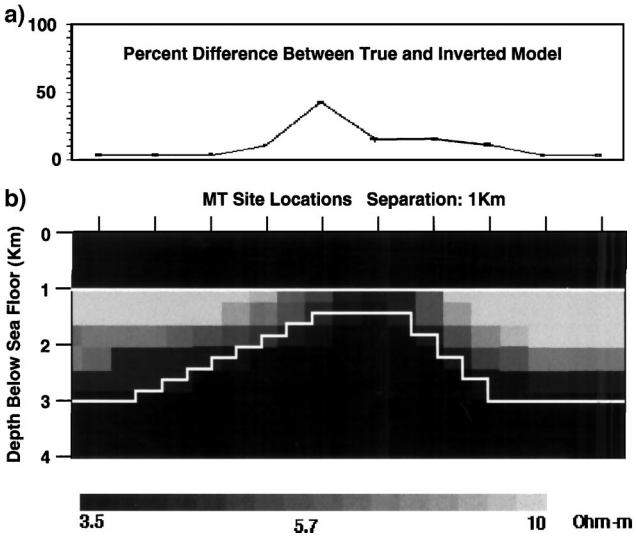

FIG. 13. Two-dimensional Occam inversion models of the TM mode only for line 3 of the model shown in Figure 11 when the model is stretched by a factor of two perpendicular to line 3. (a) Percent error in the depth of the base salt when the 3.2-ohm-m contour of the inversion model is interpreted as the base salt. (b) Occam 2-D smooth resistivity inversion of line 3 for the stretched model.

determined by marine MT. Second, resolution of the upper part of the structure (above 5 km depth) is very good, with the maximum error of 1 km below the −5 km surface location for the rooted model and about 0.5 km for the rootless model. Third, both the rooted and rootless models show anomalous low-resistivity zones (0.3 to 0.5 ohm-m) beneath the salt sill.

To demonstrate the importance of the TE mode data to model resolution, inversions of the rooted and rootless TM mode data with 5% Gaussian noise were done as before. The inversion results for the rootless model are shown in Figure 18, and the rooted inversions are shown in Figure 19. While the presence or absence of a deep root can be seen clearly in the inversions, the resolution of the salt sill between 3 and 5 km depth is much poorer without the TE data. Without the data redundancy of the TE mode, noise in the remaining TM data has a larger impact on the inverted model, causing the low-resistivity zones in the shallow part of the salt below 2.5 and 5 km on the horizontal axis. In addition, the deep root is less well defined using the TM data only.

The benefit of TE for resolving the root comes from its lack of response to the root. This at first seems contradictory until one realizes that only relatively thin (in the in-line direction) resistive roots will produce no TE response while fitting the TM response. Without the TE, the root structures can become much wider with depth and still fit the TM mode data alone.

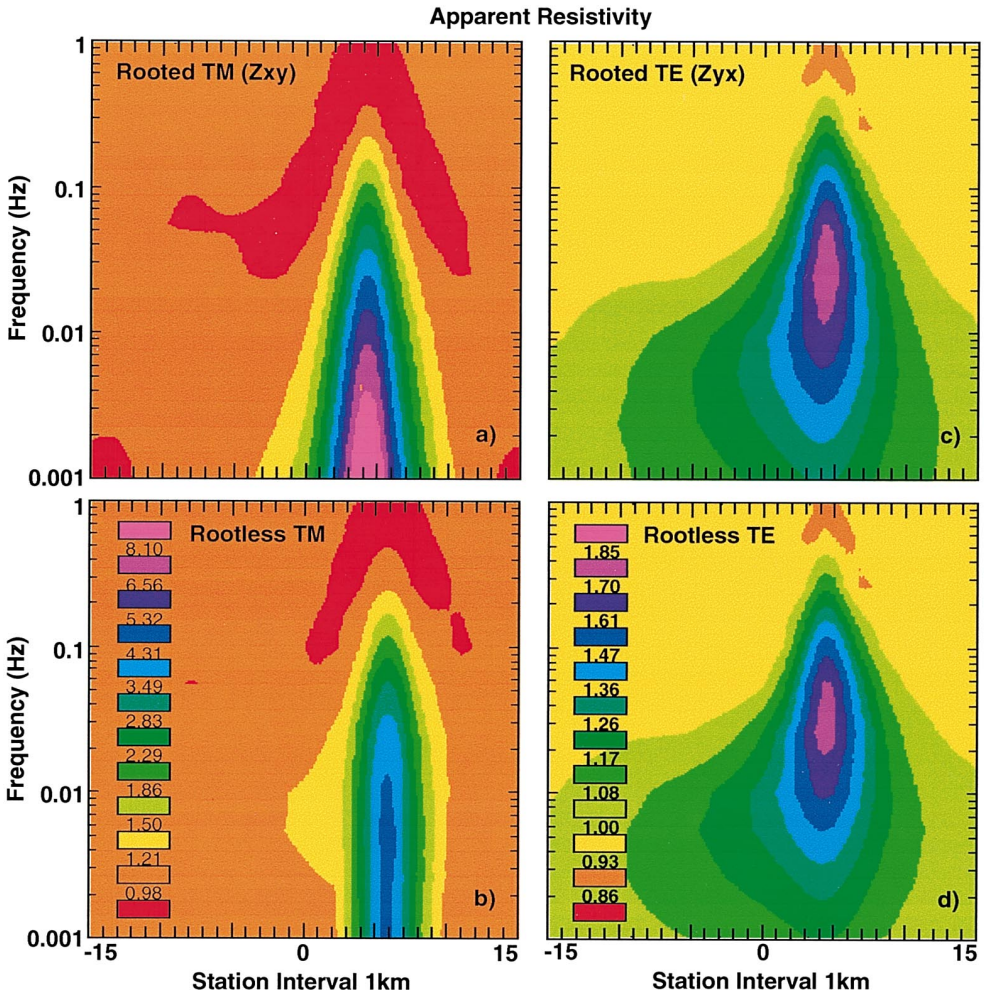

FIG. 14. TE and TM mode apparent resistivity for the salt root model with and without the root. (a) Rooted TM response. (b) Rootless TM response. (c) Rooted TE response. (d) Rootless TE response. Rooted and rootless responses use common color scales shown in the rootless panels.

2-D inversion of 3-D rooted salt structure

The question naturally arises as to the effect of strike length on the response of a structure such as the rooted model shown in Figure 16. To address this, we ran a series of 3-D versions of the rooted and rootless models where the strike length in the out-of-plane (y) direction ranged from 24 to 12 km. For this model, a strike length of 12 km represents a limit at which the 2-D inversions can distinguish the presence or absence of the root. The strike length of 12 km is approximately one-half the model's length in the observation line direction. The observation lines were at $y = 0$, with the salt extending equal amounts in the positive and negative y-directions. Figures 20 and 21 show the 2-D Occam inversion of the rootless and rooted 3-D model data, respectively. Both TE (E parallel to y) and TM (E perpendicular to y) modes were used with 5% Gaussian noise added. The 2-D inversion produces models with lower average resistivities compared to the models found for purely 2-D data. This results in the lower threshold value of 1.5 ohm-m used in the bottom panels of these plots compared to the 3.4 ohm-m used in the inversion of 2-D data. The distinction between rooted and rootless models, while present, is small and unclear evidence for the presence or absence of a root.

Three-dimensional models with a strike length of 16 km yield 2-D inversions which are significantly different and can distinguish between the rooted and rootless models. Also, if the added noise is reduced to 2% for the 12-km strike length 3-D models, the 2-D inversions yield results which would distinguish between rooted and rootless versions. Although the 2-D inversion of the 3-D rooted and rootless models with a 12-km strike length differ only slightly, the 3-D data still have significant differences between models. The TM (Z_{xy}) apparent resistivity is elevated by 25% at 0.001 Hz and 15% at 0.01 Hz by the presence of the root compared to the rootless 3-D model.

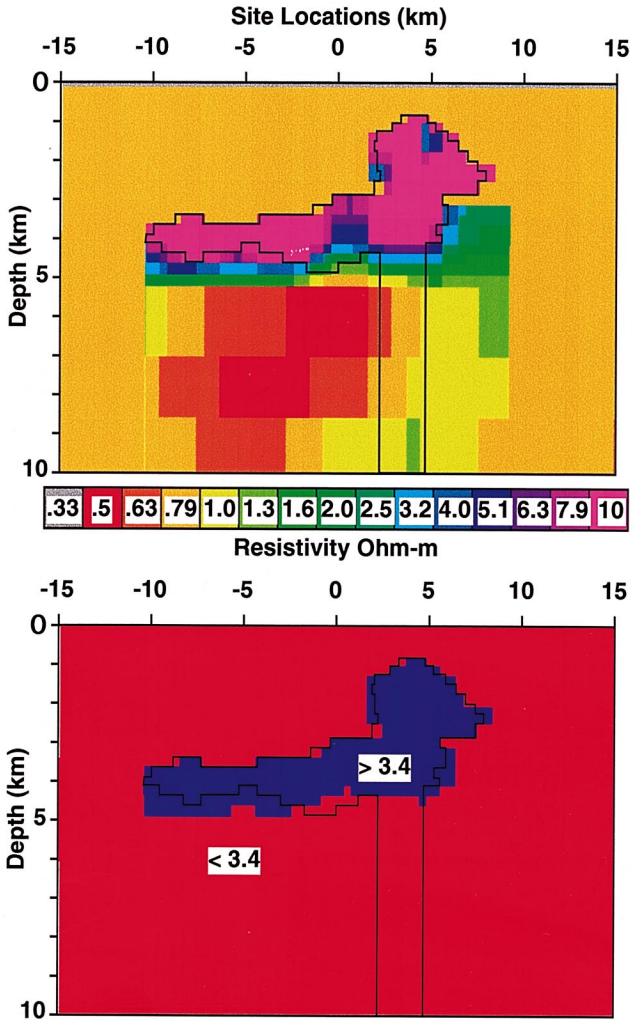

FIG. 15. Occam 2-D inversion of a 2-D salt structure without a deep root. Inversion used both TE and TM mode apparent resistivity and phase at ten frequencies evenly spaced in $\log^{10}$ between 0.001 and 1 Hz. The salt with the root is outlined in black. Sediment resistivity is 1 ohm-m; salt resistivity is 20 ohm-m. (a) Smooth inversion model resistivities. (b) Resistivities greater than 3.4 ohm-m are shown in dark blue.

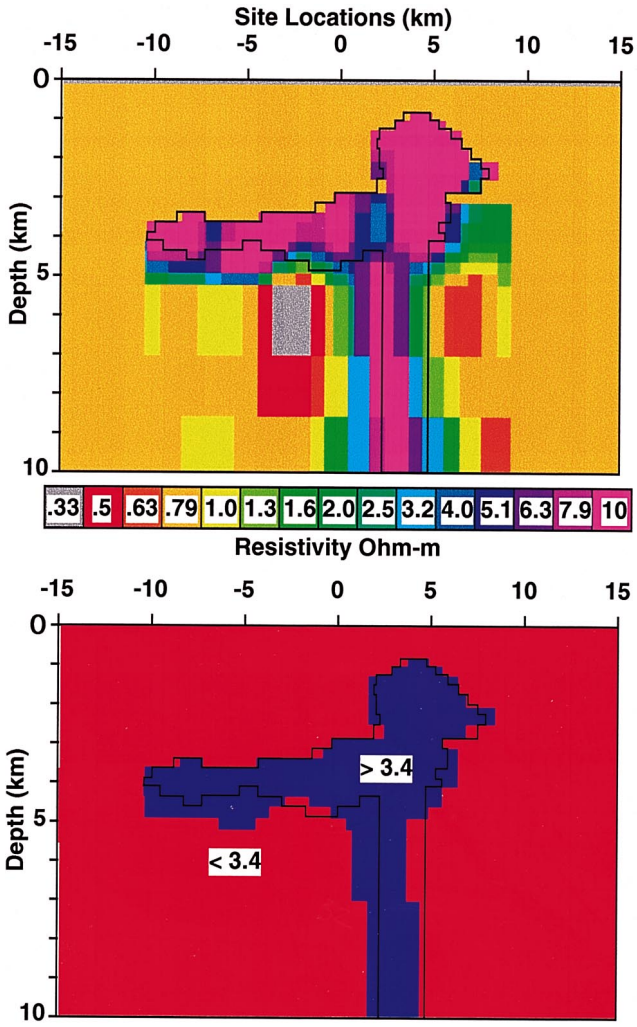

FIG. 16. Occam 2-D inversion of a 2-D salt structure with a deep root. Inversion used both TE and TM mode apparent resistivity and phase at ten frequencies evenly spaced in $\log^{10}$ between 0.001 and 1 Hz. The outline of the salt is shown in black Sediment resistivity is 1 ohm-m; Salt resistivity is 20 ohm-m. (a) Smooth inversion model resistivities. (b) Inversion model resistivities greater than 3.4 ohm-m.

We will have to wait for practical 3-D inversion to see if this difference will allow better discrimination between the rooted and rootless 3-D models than 2-D inversion affords.

COMPARISON OF POSITION ERRORS FOR 2-D MT INVERSION AND SEISMIC MIGRATION

A detailed consideration of seismic migration errors is beyond the scope of this work; however, a limited comparison of our MT inverse model errors and computed migration errors puts our results in the context of the seismic technique. Larner and Cohen (1993) and Alkhalifah and Larner (1994) provide detailed analysis of positioning errors in migration. Their papers deal primarily with migration errors induced by transversely isotropic media but also contain isotropic media as a subset. Any reader wishing to put the accuracy of our MT inversions in the context of a specific model should refer to these two papers.

As Alkhalifah and Larner (1994) state, "Most migration algorithms today are based on the assumption that the earth is isotropic, an approximation that is often not valid and thus can lead to position errors on migrated images." Given the many sources of error in field acquisition and processing which can contribute to position errors on final migrated sections, we feel it is reasonable to consider the errors induced by anisotropy alone as a minimum error estimate for migrated sections in the GOM which can be compared to the MT inversion errors.

Transverse anisotropy can be characterized by two parameters, ε and δ, defined by Thomsen (1986). Transverse anisotropy in the GOM has been noted by many authors, including Meadows and Abriel (1994) and Gonzolez et al. (1991), who have observed vertical and horizontal velocities that correspond to values of ε near 0.1. Values of δ have been observed in the range of 0.1 to 0.3 in GOM shales and near 0.0 in sands, with increasing values as a function of depth (Larner, personal communication, 1996).

As an example of vertical mispositioning of reflectors, Alkhalifah and Larner (1994) present a model consisting of horizontal reflectors with end segments having dips ranging from 30° to 90° on both sides (Alkhalifah and Larner, 1994, their Figure 10). The vertical velocity function is $v(z) = 2000 + 0.6z$ m/s with transverse isotropic parameters $\delta = -0.035$ and $\varepsilon = 0.11$, which correspond to the Taylor sandstone (Thomsen, 1986). When the data are migrated with an isotropic depth migration algorithm (Alkhalifah and Larner, 1994, their Figure 13), the reflectors are imaged too deep. The 1.25-km reflector is approximately 3.5% too deep, while the 3.0-km reflector is approximately 6.5% too deep. The base salt positioning errors in the 2-D MT inversion of the anticline model

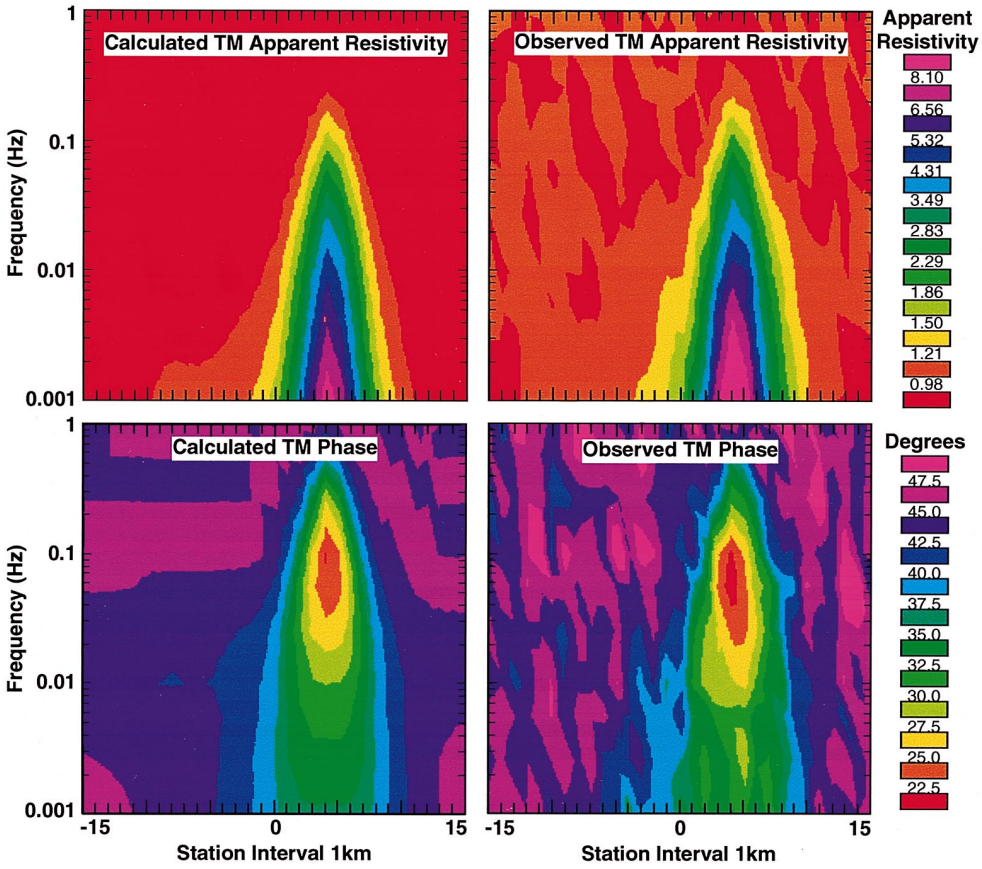

FIG. 17. Observed and computed TM apparent resistivities and phase for the rooted salt body shown in Figure 16. (a) Calculated TM apparent resistivity for the inverse model shown in the top of Figure 16. (b) Observed TM apparent resistivity with 5% random noise. (c) Calculated TM phase for the inverse model shown in the top panel of Figure 16. (d) Observed TM phase with 5% random noise added.

(Figure 9) range from 5% on the flanks where the structure is horizontal to 14% at the apex of the anticline.

Horizontal positioning of near-vertical reflectors in migration has inherently more uncertainty than vertical positioning. If we consider the horizontal position of the edges of the deep salt root shown in Figure 16 in the depth range of 5 to 9 km, this corresponds to a two-way time range of 2.8 to 3.8 s for the $v(z) = 2000 + 0.6z$ m/s velocity function. Alkhalifah and Larner (1994) present the position error as a function of dip angle for two-way times of 1, 2, 3, and 4 s for $\varepsilon = 0.1$ and a range of δ. They plot the position errors as a function of horizontal wavelength after migration. We have used a slope [p in equation (16) of Larner and Cohen (1993)] of 0.75 s/km as appropriate for the GOM, taken from Figure 7a of Hale et al. (1992), to compute the horizontal wavelength before migration to convert values from Alkhalifah and Larner (1994, their Figure 6) into meters. Figure 22 shows the lateral position errors after migration for a vertical reflector (dip = 90°) for $\delta = 0.0$, appropriate for sand, and $\delta = 0.1$, appropriate for shale at dominant frequencies of 20 and 30 Hz. The figure shows that the lateral position errors in the shallower section around 1 s two-way time are small—on the order of 50 m. However, at a two-way time of 3 s an error near 350 m results in shale; an error of 200 m results in sand at 30 Hz. At 4 s the error in shale at 20 Hz is nearly 1 km. The migration errors from Figure 22 at the top of the root structure (two-way time of 3 s) shown in Figure 15 are less than half the error in the horizontal position of the left side of the root from the MT inversion. However, the errors in migration and the accuracy of MT become comparable at the base of the structure. This comparison strongly suggests that a joint inversion of seismic and MT, each depending on different physical properties, would yield more accurate locations for subsalt structures.

In many exploration situations where well data are available, migration parameters can be tuned more finely by trial and error, resulting in more accurate migrations than the examples

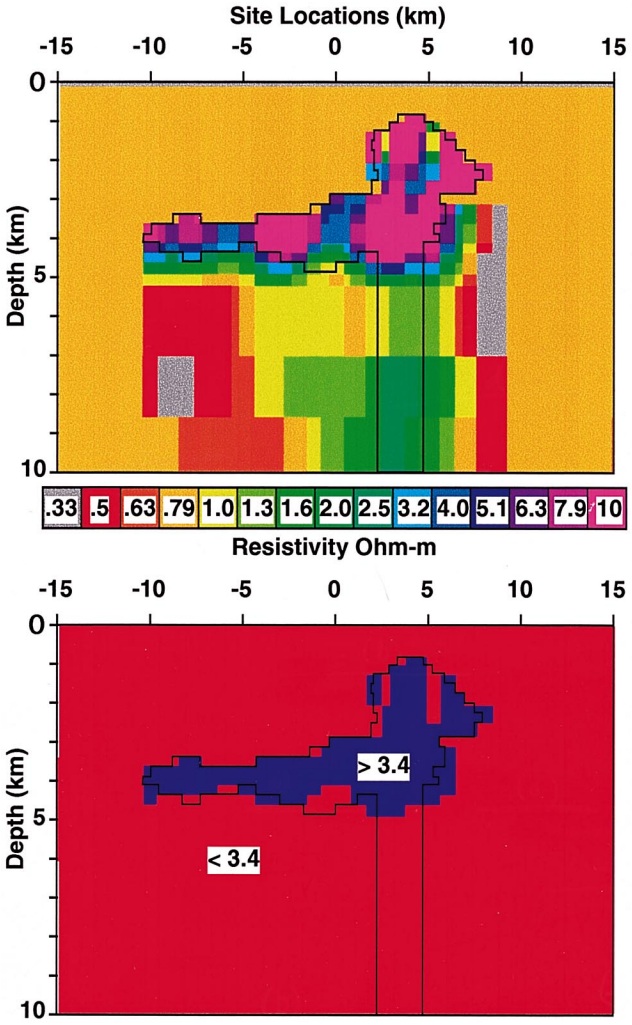

FIG. 18. Occam 2-D inversion of a 2-D salt structure without a deep root. Inversion used only TM mode apparent resistivity and phase at ten frequencies evenly spaced in $\log^{10}$ between 0.001 and 1 Hz. The salt with the root is outlined in black. Sediment resistivity is 1 ohm-m; salt resistivity is 20 ohm-m. (a) Smooth inversion model resistivities. (b) Resistivities greater than 3.4 ohm-m are shown in dark blue.

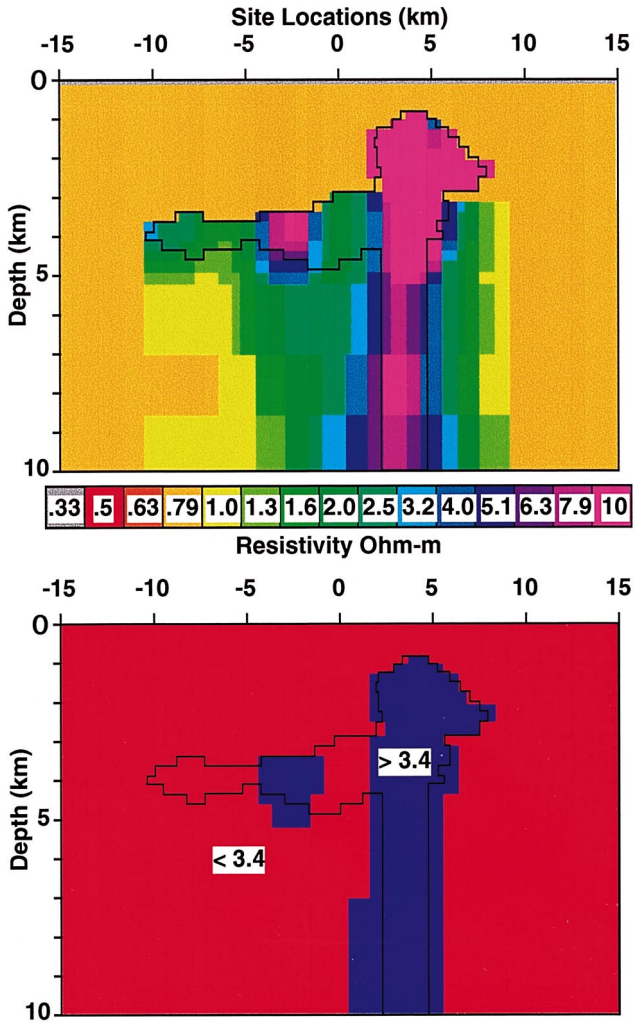

FIG. 19. Occam 2-D inversion of a 2-D salt structure with a deep root. Inversion used only TM mode apparent resistivity and phase at ten frequencies evenly spaced in $\log^{10}$ between 0.001 and 1 Hz. The salt is outlined in black. Sediment resistivity is 1 ohm-m; salt resistivity is 20 ohm-m. (a) Smooth inversion model resistivities. (b) Inversion model resistivities greater than 3.4 ohm-m.

considered here. However, these examples can be considered within the range of errors expected in the GOM for rank exploration where no other data exist. Furthermore, in rank explorations it is unlikely that full 3-D data and prestack-depth migration would be used. In rank exploration where knowledge of transverse anisotropy is not available, the information available from MT regarding salt-sediment contacts is expected to be similar to that provided by reconnaissance 2-D seismic.

FUTURE WORK

The current work is far from a complete study of the potential application of marine MT for mapping salt or any high-velocity, high-resistivity structure. The current study highlights the difficulties of using smooth inverse models to interpret sharp discontinuities in physical properties, such as occur in resistivity at salt-sediment contacts. A better approach would be to use an inversion scheme that includes the ability to accommodate sharp discontinuities in the inverse model. Work is currently under way to refine a new 2-D MT inverse algorithm parameterized by variable thickness layers and polygonal regions whose boundary locations are the inverse parameters. Additionally, there is a need for 3-D MT inversion capabilities.

CONCLUSIONS

Based on numerical modeling, marine MT can map the base of anticlinal features in lateral salt intrusions to within an average depth accuracy of better than 10%. Vertical resolution on salt thickness is lost for salt thinner than approximately one-tenth of a plane wave skin depth at the highest frequency that responds to the salt presence. The lateral resolution is comparable to the vertical resolution. Different slopes on the opposite sides of the model anticlines were clearly mapped by the 2-D inversions. The maximum errors in salt anticline thickness occur for both 1-D and 2-D MT inversions at the apex of anticlines where the salt thickness was only 400 m. Two-dimensional MT inversion using both TE and TM modes resolves the anticline

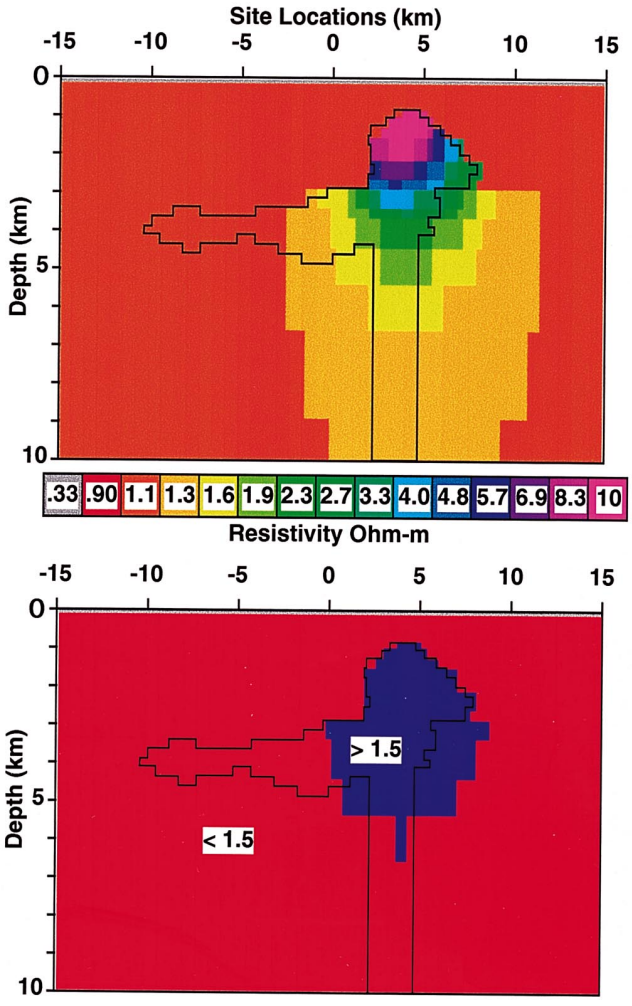

FIG. 20. Occam 2-D inversion of a 3-D salt structure without a deep root. The structure is 12 km long in the out-of-plane direction. The observed data are from a line at the midpoint in the bodies' strike extent. Inversion used TE (Z_{yx}) and TM (Z_{xy}) mode apparent resistivity and phase at ten frequencies evenly spaced in $\log^{10}$ between 0.001 and 1 Hz. The salt with the root is outlined in black. (a) Smooth inversion model resistivities. (b) Resistivities greater than 1.5 ohm-m are shown in dark blue.

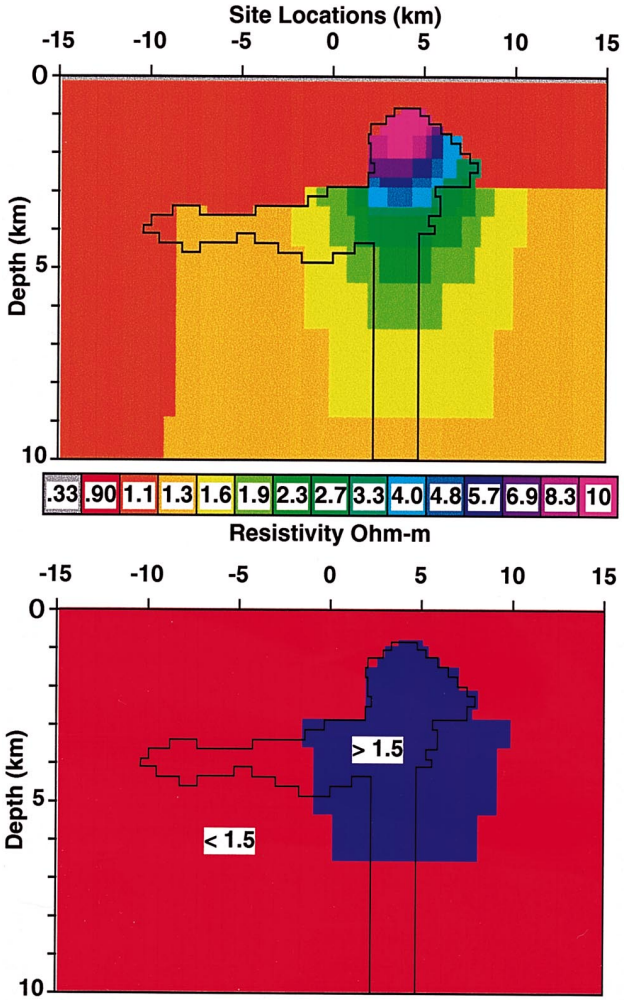

FIG. 21. Occam 2-D inversion of a 3-D salt structure with a deep root. The structure is 12 km long in the out-of-plane direction. The observed data are from a line at the midpoint in the bodies' strike extent. Inversion used TE (Z_{yx}) and TM (Z_{xy}) mode apparent resistivity and phase at ten frequencies evenly spaced in $\log^{10}$ between 0.001 and 1 Hz. The salt with the root is outlined in black. (a) Smooth inversion model resistivities. (b) Resistivities greater than 1.5 ohm-m are shown in dark blue.

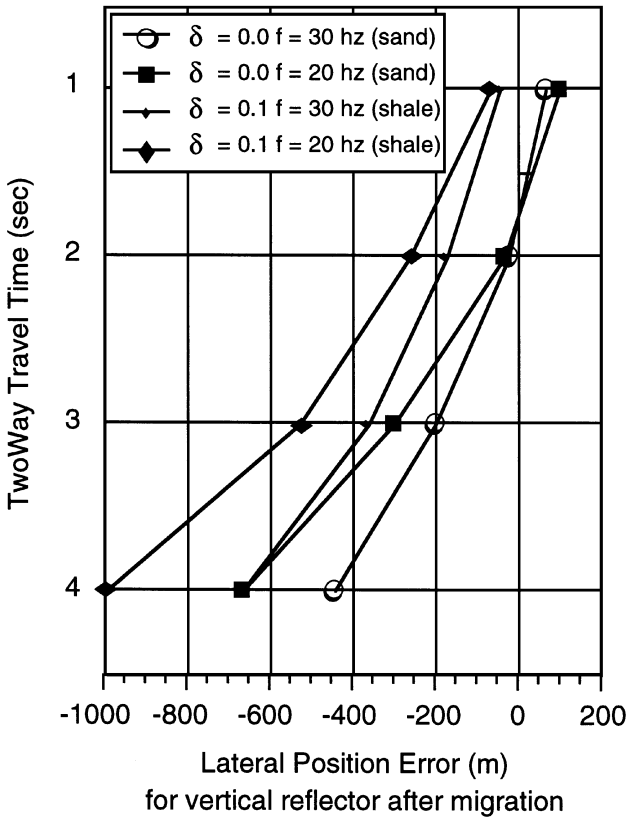

FIG. 22. Lateral positions errors for a vertical reflector when velocity anisotropy is neglected in migration. Taken from Alkhalifah and Larner (1994, their Figure 6) for $\delta = 0.0$, appropriate for sand, and $\delta = 0.1$, appropriate for shale at dominant frequencies of 20 and 30 Hz. Vertical velocity function: $v(z) = 2000 + 0.6z$ m/s velocity. A slope [p in equation (16) of Larner and Cohen (1993)] of 0.75 s/km, taken from Figure 7a of Hale et al. (1992), was used to compute the horizontal wavelength before migration to convert values from Alkhalifah and Larner's Figure 6 (1994) into meters.

apex thickness to within 14%. Two-dimensional inversion of 3-D numerical data indicates that as long as the horizontal aspect ratio of a 3-D anticline is greater than two, the inversion accuracy is comparable to the accuracy of inverting truly 2-D data except at the apex. Three-dimensional anticline thickness estimates via 2-D inversion of TM mode data at the apex is comparable to the accuracy of 2-D inversion of truly 2-D data using only the TM mode. Although the quantitative measure of picking a single resistivity contour produced roughly 50% errors at the apex for the 3-D model, resistivities were reduced compared to the areas of thicker salt on either side, giving a qualitative measure of the salt thinning. Finally, the marine MT data can distinguish between those models which possess a deep root structure and those which do not.

The most important conclusion from this study is that MT can provide valuable complementary data to resolve velocity ambiguities that cause significant positioning errors in migrated seismic data. The fact that realistic anisotropies can cause mispositioning errors which are a significant fraction of MT inversion errors indicates that if the two data sets were interpreted together, the absolute error in the location of interfaces could be reduced.

ACKNOWLEDGMENTS

We would like to thank corporate sponsors AGIP, BP, BHP, British Gas, Chevron, Texaco, and Western Atlas in cooperation with the U.S. Dept. of Energy, Office of Energy Research, Office of Computational and Technology Research, Laboratory Technology Applications Division, under Contract No. DE-AC03-76SF00098.

REFERENCES

Alkhalifah, T., and Larner, K., 1994, Migration error in transversely isotropic media: Geophysics, **59**, 1405–1418.
Chave, A. D., Constable, S. C., and Edwards, R. N., 1991, Electrical exploration methods for the seafloor, *in* Nabighian, M. N., Ed., Electromagnetic methods in applied geophysics, 2: Soc. Expl. Geophys., 931–969.
Constable, S. C., Cox, C. S., and Chave, A. D., 1986, Offshore electromagnetic surveying techniques: 56th Ann. Internat. Mtg., Soc. Expl. Geophys., Expanded Abstracts.
Constable, S. C., Parker, R. L., and Constable, C. G., 1987, Occam's inversion—a practical algorithm for generating smooth models from electromagnetic sounding data: Geophysics, **52**, 289–300.
Edwards, R. N., 1988, Two-dimensional modeling of a towed in-line electric dipole-dipole sea-floor electromagnetic system—the optimum time delay or frequency for target resolution: Geophysics, **53**, 846–853.
Gamble, T. D., Goubau, W. M., and Clarke, J., 1979, Magnetotellurics with a remote magnetic reference: Geophysics, **44**, 53–68.
Gonzalez, A., Lynn, W., and Robinson, W. F., 1991, Prestack frequency-wavenumber (f-k) migration in transversely isotropic media: 61st Ann. Internat. Mtg., Soc. Expl. Geophys., Expanded Abstracts, 1155–1157.
deGroot-Hedlin, C., and Constable, S., 1990, Occam's inversion to generate smooth, two-dimensional models from magnetotelluric data: Geophysics, **55**, 1613–1624.
Hale, D., Hill, N. R., and Stefani, J., 1992, Imaging salt with turning seismic waves: Geophysics, **57**, 1453–1462.
Hoehn, G. L., and Warner, B. N., 1960, Magnetotelluric measurements in the Gulf of Mexico at 20m ocean depths, *in* Handbook of geophysical exploration at sea: CRC, 397–416.
Hoversten, G. M., 1992, Seaborne electromagnetic subsalt exploration: EOS, **73**, No. 43, Suppl., 313.
Hoversten, G. M., and Unsworth, M., 1994, Subsalt imaging via seaborne electromagnetics: Proc. Offshore Tech. Conf., **26**, 231–240.
Larner, K. L., and Cohen, J. K., 1993, Migration error in transversely isotropic media with linear velocity variation in depth: Geophysics, **58**, 1454–1467.
Mackie, R. L., Madden, T. R., and Wannamaker, P. E., 1993, Three-dimensional magnetotelluric modeling using difference equations—Theory and solutions: Geophysics, **58**, 215–226.
Meadows, M. A., and Abriel, W. L., 1994, 3-D poststack phase-shift migration in transversely isotropic media: 64th Ann. Internat. Mtg., Soc. Expl. Geophys., Expanded Abstracts, 1205–1208.
Smith, J. T., and Booker, J. R., 1988, Magnetotelluric inversion for minimum structure: Geophysics, **53**, 1565–1576.
Thomsen, L., 1986, Weak elastic anisotropy: Geophysics, **51**, 1954–1966.
Torres-Verdin, C., and Bostick, F. X., Jr., 1992, Principles of spatial surface electric field filtering in magnetotellurics: Electromagnetic array profiling (EMAP): Geophysics, **57**, 603–622.
Wannamaker, P. E., Stodt, J. A., and Rijo, L., 1987, A stable finite-element solution for two-dimensional magnetotelluric modeling: Geophys. J. Roy. Astr. Soc., **88**, 277–296.
Vozoff, K., 1991, The magnetotelluric method, *in* Nabighian, M. N., Ed., Electromagnetic methods in applied geophysics, 2: Soc. Expl. Geophys., 641–711.